PCCP

Accepted Manuscript

ROYAL SOCIETY OF CHEMISTRY

www.rsc.org/pccp

Physical Chemistry Chemical Physics
CREATED USING THE RSC LaTeX PCCP ARTICLE TEMPLATE – SEE www.rsc.org/electronicfiles FOR DETAILS
ARTICLE TYPE www. rsc.org/xxxxxx | XXXXXXXX

Dynamics of Actinyl Ions in Water: A Molecular Dynamics Simulation Study

Surya Prakash Tiwari[a], Neeraj Rai[a,b] and Edward J. Maginn[a,*]

Received Xth XXXXXXXXXX 20XX, Accepted Xth XXXXXXXXX 20XX
First published on the web Xth XXXXXXXXXX 200X
DOI: 10.1039/b000000x

The dynamics of actinyl ions (AnO_2^{n+}) in aqueous solutions is important not only for the design of advanced separation processes but also for understanding the fate of actinides in the environment. The hazardous nature of actinides makes it difficult to measure transport and thermodynamic properties experimentally, so predictive simulations are an attractive method for studying these systems. Here, we report the results of atomistic-level molecular dynamics simulations of actinyl ions (of U, Np, Pu, and Am) in their mono- and dication states in aqueous solution. Quantum mechanically derived force field parameters are used to compute self-diffusion coefficients of the actinyl ions, water exchange mechanisms, and residence times of water molecules in the first solvation shell of the actinyl ions. We find that monocation actinyl ions diffuse slightly faster than their dication counterparts. Our simulations suggest that there are two distinct water exchange mechanisms for mono and dications. An associative interchange pathway is observed for water exchange involving dication actinyls, while in monocation actinyls the exchange occurs via a dissociative mechanism. The residence time of water molecules in the first solvation shell depends on the water exchange mechanism. In the case of dications, a stiffer actinyl bond angle results in a longer residence time, while for monocations, a shorter water coordination distance leads to a longer residence time. The simulations predict much faster water exchange for UO_2^{2+} than what is observed experimentally with NMR, but other properties are consistent with experiments.

1 Introduction

With large amounts of radioactive waste stored in various underground storage tanks, the environmental impact of any discharge of these material can be catastrophic. The storage of used nuclear fuel in geological repositories is either already implemented in some parts of the world or under consideration for closing the nuclear fuel cycle. Clearly, understanding the transport properties of key actinide elements (one of the main constituents of radioactive waste) is of paramount importance. Furthermore, dynamic properties of actinyl ions need to be known for designing advanced separation processes used in recycling. Along with the transport properties, understanding the mechanism of the exchange between coordinated and free solvent can help us better understand actinide ligand chemistry.[1]

The uranyl dication (UO_2^{2+}) is the most widely studied actinyl species in large part because uranium is the majority actinide component in fuel and waste streams. Experimental and computational studies on UO_2^{2+} have been performed to determine its dynamic properties, viz. diffusion coefficient, residence time and mechanism of water exchanges between coordinated and free water.[1–21] However, there are several discrepancies in the literature. For example, theoretical models based on experimental ionic conductivity measurements have suggested that the diffusion coefficients for monocation actinyls are roughly twice that of the dication actinyls, though this is contrary to direct experimental measurements.[2,3] The residence time for water exchange of UO_2^{2+} has been observed in NMR experiments to be of the order of 10^{-6} s, whereas simulations[14,22] suggest that it is much faster, on the order of 10^{-9} s. Recently, Kerisit et al.[21] developed a new model for classical simulation of UO_2^{2+} in water to accurately reproduce the residence times observed experimentally with NMR, but the first hydration shell of UO_2^{2+} in their model was tighter than what has been observed experimentally.[23–26]

With a goal to develop a force field for modeling actinide systems in a consistent manner, we reported a general procedure for determining intermolecular interaction parameters from quantum mechanical calculations.[27] Using this procedure, we developed force field parameters for classical simulations of actinyl ions (UO_2^{n+}, NpO_2^{n+}, PuO_2^{n+}, and AmO_2^{n+} ($n = 1,2$)) in water.[28] The model was shown to give good "static" results for water coordination numbers, hydration radii, actinyl ion structure, and solvation free energies. In the present work, we test the ability of this model to reproduce dynamical properties by carrying out molecular dynam-

[a] *Department of Chemical and Biomolecular Engineering, University of Notre Dame, 182 Fitzpatrick Hall, Notre Dame, IN 46556, USA. Fax: 01 574 631 8366; Tel: 01 574 631 5687; E-mail: ed@nd.edu*
[b] *Dave C. Swalm School of Chemical Engineering, Mississippi State University, Mississippi State, MS, USA 39762*

ics (MD) simulations of the transport properties and ligand exchange dynamics of actinyl ions in water. Self-diffusion coefficients, residence times and water exchange mechanisms have been studied for each of the eight actinyl ions in non-polarizable SPC/E water.[29] Further, to see the impact of different water models on the dynamics, UO_2^{2+} has been chosen to study these properties in water modeled with the SPC/Fw,[30] TIP3P,[31] TIP4P,[31] and TIP5P[32] potentials. In keeping with the definition from previous work[28], UO_2^{2+} modelled with these other water models will be referred to as the "hybrid" UO_2^{2+} model.

2 Simulation Details

Inter- and intramolecular force field parameters were taken from our previous work[28]. The system consisted of one actinyl ion and 1000 water molecules in a cubic box of ∼3.12 nm length, with periodic boundary conditions applied in all directions. A time step of 0.002 ps was used for all the rigid water models (SPC/E, TIP3P, TIP4P, TIP5P), while 0.001 ps was used for simulations with the flexible SPC/Fw water model. The leap-frog algorithm was used for integrating the equations of motion. Single precision Gromacs 4.5.5[33] was used for all the MD simulations. The simulations were performed in the NVT ensemble at $T = 298.15$ K using a weak Nosé-Hoover thermostat[34] with a time constant of 6 ps. It has been shown that the use of the Nosé-Hoover thermostat does not perturb the dynamical properties of such systems[35]. The production runs were 150 ns long. The initial 5 ns of data from the simulations were discarded before collecting averages. Trajectories were saved with a frequency of 0.25 ps for analysis. In addition, shorter simulations of 5 ns were also carried out to visualize the water exchange mechanisms, where trajectories were saved with a frequency of 0.02 ps.

The analysis program g_msd available in the Gromacs 4.5.5 suite was used to calculate self-diffusion coefficients, while in-house programs were used to compute residence times and examine the water exchange mechanisms. VMD[36] was used to visualize the trajectories. All properties were calculated from five independent simulations, with the standard deviation taken as the uncertainty.

3 Results and Discussions

3.1 Self-Diffusion Coefficients

Self-diffusion coefficients D_A of particles of type A were obtained from the long-time slope of the mean squared displacement (MSD) via the Einstein relation[37]

$$6D_A t = \lim_{t\to\infty} \langle |\mathbf{r}_i(t) - \mathbf{r}_i(0)|^2 \rangle_{i\in A} \qquad (1)$$

where, $\mathbf{r}_i(t)$ is the position vector of the i^{th} particle at time t. 50 ps of time differences were used as reference points for MSD calculations. Diffusion coefficients of AnO_2^{n+} were calculated from the slopes of the MSD plots in the time interval from 200 ps to 2000 ps, where the MSD was confirmed to be linear.

MSD plots and self-diffusion coefficients of all AnO_2^{n+} ions in SPC/E water are shown in Fig. 1 and Table 1, respectively. Note that these results have not been corrected for finite system size, and so actual values will be slightly higher (by up to 10 percent).[38,39] Actinyl ions with +1 charge have slightly higher self-diffusivities than those with a +2 charge, but the difference is minor. It is reasonable to expect that all the ions have nearly the same self-diffusivity because each actinyl ion, regardless of whether it is a mono- or dication, has a coordination shell of five water molecules that persists over time scales commensurate with diffusion times. The fact that monocations have diffusivities slightly larger than dications is because the monocations bind water slightly less strongly than the dications, which, in general, leads to increased water exchange (shown in Section 3.3) and, hence, faster dynamics. The relative binding strength of the ions with water can be observed in radial distribution function (RDF) plots in our previous work.[28] In a given charge state, the ions have very similar mobilities.

Table 1 shows a comparison of simulated self-diffusivities and those determined experimentally using direct[2,3] and indirect (by measuring ionic conductivities and mobilites[4–7]) methods. In the direct methods for UO_2^{2+} and UO_2^{+}, diffusion current constants were measured and directly related to the diffusion coefficient via the Ilkovic equation[2]. The direct measurements of NpO_2^{2+} and PuO_2^{2+} utilized a capillary tube diffusion cell[3]. These results generally agree with those obtained from the simulations reported in the present work. Previous MD simulations of aqueous UO_2^{2+} by Kerisit et al.[22] using a force field from Wipff and co-workers[41,42] resulted in a UO_2^{2+} diffusivity of 0.7659×10^{-9} m^2/s which is somewhat higher than our predictions and the direct experimental measurements.

Self-diffusivities can also be determined indirectly by measuring the ionic conductivity Λ and applying the Nernst-Einstein equation[43]

$$\Lambda = \frac{F^2}{RT}\left(\nu_+ z_+^2 D_+ + \nu_- z_-^2 D_-\right)(1-\Delta) \qquad (2)$$

where ν_i and z_i are stoichiometric and charge numbers, respectively, and F is the Faraday constant. The parameter Δ is a so-called "deviation parameter" and is typically neglected, though formally it is zero only for an infinitely dilute system where the ions have no interaction with each other. The indirect measurements of UO_2^{2+} diffusivities, discussed in detail by Kerisit et al.[22], range from 0.426×10^{-9} m^2/s to

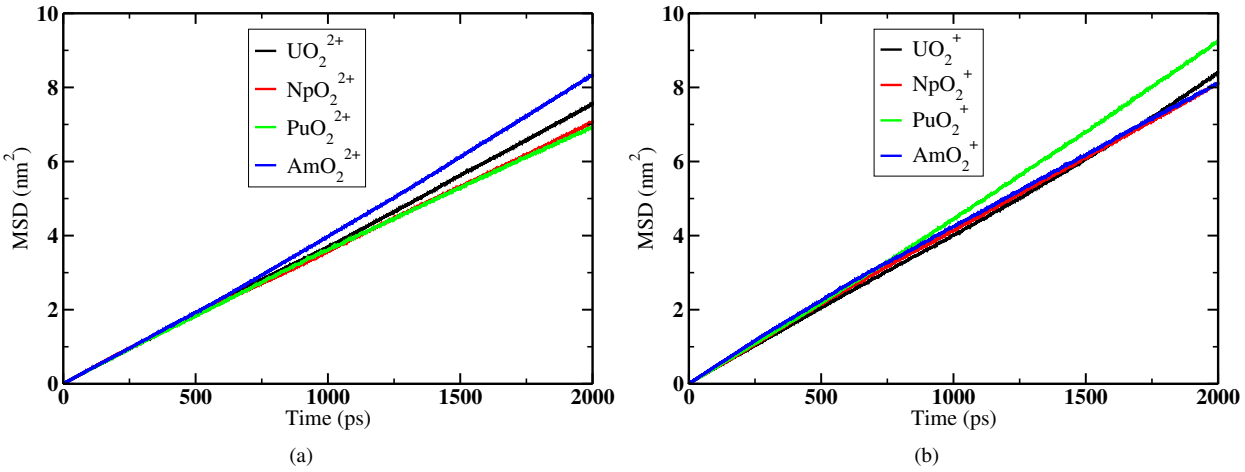

Fig. 1 MSD as a function of time for AnO_2^{2+} and AnO_2^{+} in SPC/E water. Slope of log-log plots of these MSD lines are within 0.9 to 1.1.

0.759×10^{-9} m^2/s.[4–7]

Mauerhofer et al.[40] carried out a theoretical study of actinyl dynamics in which they developed a simplified geometric model of the actinyl ions and invoked the Stokes-Einstein law with various assumptions. They first calculated the limiting ionic conductivity of actinyl ions, and then used a form of the Nernst-Einstein relation to calculate diffusion coefficients. Their model yielded an estimate for all the dications on the order of 0.7×10^{-9} m^2/s and so are in reasonable agreement with our simulations. Their estimates of the diffusivity of the monocations, however, are all on the order of 1.4×10^{-9} m^2/s which is around double that obtained from MD simulations and from direct experimental measurements. Mauerhofer et al. have also used experimental values of limiting ionic conductivities and ionic mobilities to calculate diffusion coefficients, which are shown in Table 1 as $D_{\mathrm{Exp.}}^{\mathrm{Indirect}}$. These results approximately match what they have obtained via their theoretical model.

The reason that the theoretical model predicts that the monocation diffusivites are about twice that of the dications stems from the fact that the experimental conductivities are roughly equal for all the ions. If $\Delta = 0$ in Eq. 2, then the diffusivities of the less charged ions must be greater. However, it is highly unlikely that there is no association of ions in these systems, and in fact the dications will tend to have larger values of Δ than the monocations. This, combined with the finding in the present work that the solvation environment around the different actinyl ions is similar, suggests that the indirect diffusivity estimate for UO_2^+ in Table 1 may be too high.

3.2 Water Exchange Mechanism

The water exchange mechanism can be interpreted in terms of classical ligand exchange mechanisms,[44] for which there are three stoichiometrically distinct types: a dissociative path (**D**) where a leaving water is lost in the first step, producing an intermediate of reduced coordination number; an associative (**A**) path in which an entering water molecule joins the first solvation shell of the ion, resulting in an intermediate of increased coordination number; and a so-called "interchange" path (**I**) where the leaving water molecule moves from the inner to the outer coordination sphere in a concerted manner with the entering water molecule, which moves from the outer to inner coordination sphere. Often the **I** path is further broken down into "associative interchange" ($\mathbf{I_a}$) and "dissociative interchange" ($\mathbf{I_d}$) pathways. In the $\mathbf{I_a}$ classification, there is substantial bonding between the entering and leaving water molecules, with the entering water molecule playing a role in the kinetics of exchange. In the $\mathbf{I_d}$ mechanism, the bonding between the entering and leaving water molecules is much weaker and the entering water molecule plays little role in the kinetics of exchange. These distinctions are somewhat arbitrary, but simply serve to provide a qualitative picture of exchange[44–48].

The MD simulations provide insight into the exchange mechanism whereby bound equatorial water molecules exchange with bulk water. Pomogaev et al.[28] have shown that all the actinyl ions are coordinated with five water molecules in equilibrium. The time dependence of the total number of water molecules in the first hydration shell of the actinyl ions is shown in Fig. 2 over three different time scales. The number of water molecules in the first hydration shell fluctuates as there are abrupt transitions due to water exchange. The "dominant" transient for the dication actinyls is an associative (**A**) mechanism in which the coordination number goes from $5 \rightarrow 6 \rightarrow 5$, while for the monocation actinyls it is a dissociative (**D**) mechanism in which the coordination numbers during exchange are

Table 1 Self-diffusion coefficients (D, $10^{-9}m^2s^{-1}$) of AnO_2^{n+} computed in SPC/E water from MD simulations, and compared with experimental results. Subscripts refer to uncertainties in the last digit(s); for e.g. 0.61_9 is equivalent to 0.61 ± 0.09, 0.64_{10} is equivalent to 0.64 ± 0.10.

AnO_2^{n+}	D^a_{MD}	$D^{Direct}_{Exp.}$	$D^{Indirect\ d}_{Exp.}$
UO_2^{2+}	0.61_9	0.68^b	$[0.426$ to $0.759_{27}]^e$
NpO_2^{2+}	0.64_{10}	$\sim 0.8^c$	–
PuO_2^{2+}	0.61_8	$\sim 0.55^c$	0.786_{27}
AmO_2^{2+}	0.6_1	–	–
UO_2^{+}	0.68_6	0.70^b_{02}	1.411_{53}, 1.358_{80}
NpO_2^{+}	0.70_8	–	–
PuO_2^{+}	0.68_8	–	–
AmO_2^{+}	0.8_1	–	–

[a] This work– from MSD calculations. [b] From Ref. 2. [c] Diffusion coefficient value is estimated for 0.056 molar ions from a plot of diffusion coefficient vs. concentration given in the work of Marx et al.[3] [d] Mauerhofer et al.[40] calculated these diffusion coefficients from ionic conductivity and ionic mobility experiments using the Nernst-Einstein relation. [e] Kerisit et al.[22] further looked at the reported experimental ionic conductivity and ionic mobility results of UO_2^{2+} and converted them into the diffusion coefficients using the Nernst-Einstein relation.

mainly $5 \rightarrow 4 \rightarrow 5$. Though di- and monocation actinyls also have transient states with four and six water molecules in the first hydration shell, respectively, these transient states are observed much less often. The rates of formation of "dominant" transient states for the water to be exchanged is directly related to the residence time, which is discussed in the next section.

Further insight into the exchange process of water between the first and the outer coordination shells of dication actinyls can be obtained by examining snapshots of intermediate states. Fig. 3 shows four representative snapshots from a simulation in which water exchange occurs for UO_2^{2+}. Similar behavior is observed for other dications. Fig. 3 (c) shows that an associative complex $[UO_2(H_2O)_6]^{2+}$ forms, in which the oxygen atoms of the entering and leaving water molecules are at approximately 0.27 nm from the U atom. This distance is slightly more than the nominal coordination distance of $\approx$ 0.246 nm[28], but is less than the extent of the first hydration shell ($\approx$0.30 nm)[28]. Also notice that UO_2^{2+} is significantly bent in Fig. 3 (c), which suggests that the entering water molecule changes the conformation of the ion and that the stiffness of the O-An-O bond is important in the exchange process. As shown below, the stiffness of this angle does indeed play a role in the exchange kinetics. The exchange mechanism

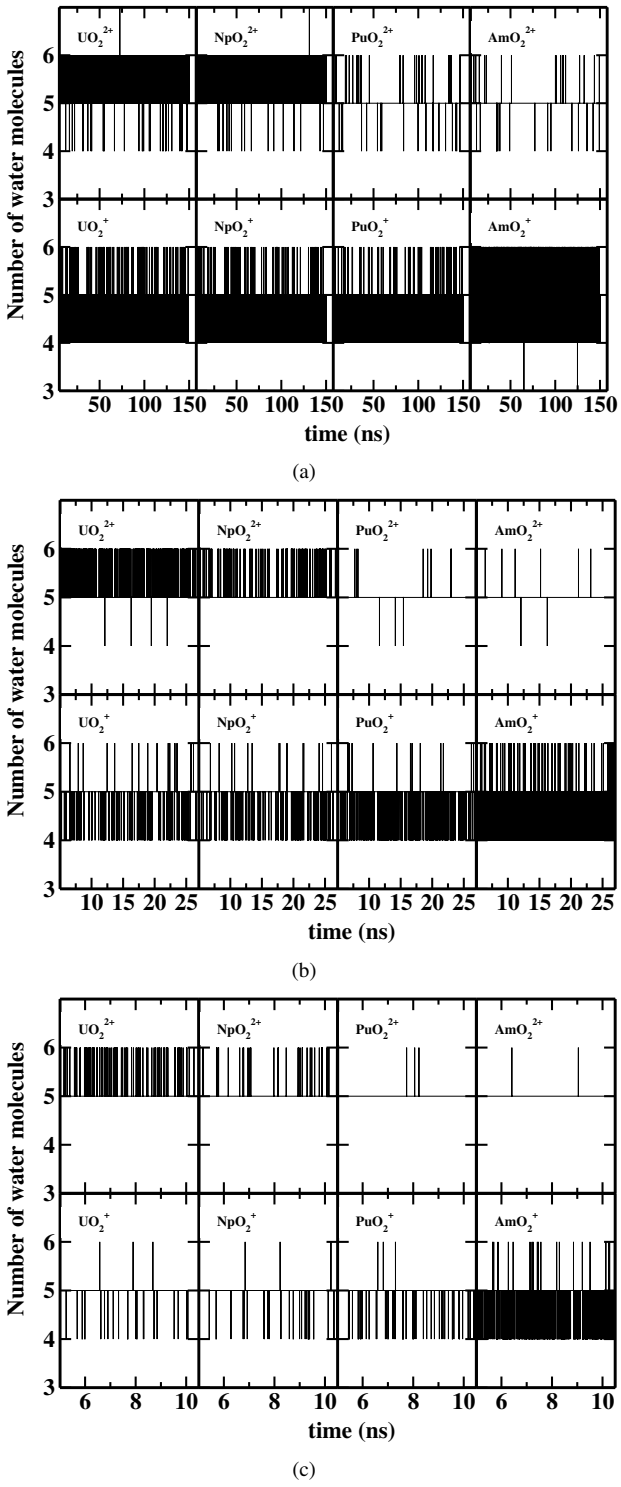

Fig. 2 Total number of water molecules in the first hydration shell of actinyl ions vs. time, shown in three different time scale resolutions.

shown in Fig. 3 was the dominant mechanism observed in the simulations, and therefore we conclude that the dication water exchange mechanism can be classified as $\mathbf{I_a}$ as defined in the schematic transition states shown in the literature.[44–48]

Water exchange for UO_2^{2+} has been studied previously by Vallet et al.[8] and others[1,10,12,14–20,49]. They ruled out the possibility of **D** exchange, but couldn't distinguish between **A** or $\mathbf{I_a}$ exchange mechanisms, because both pathways involve a coordination complex containing six water molecules ($[UO_2(H_2O)_6]^{2+}$). Vallet et al.[9] also studied the water exchange mechanisms for NpO_2^{2+} and PuO_2^{2+} using quantum calculations. They concluded that these dications follow the $\mathbf{I_a}$ mechanism. Using NMR experiments, Bardin et al.[18] suggested that the $\mathbf{I_a}$ mechanism is operative for UO_2^{2+}, NpO_2^{2+} and PuO_2^{2+}. The results of the present work are consistent with these other studies, and suggest that the primary water exchange mechanism for dication actinyl ions is associative interchange.

In contrast to the dication actinyls, the monocation actinyls tend to exchange water via a dissociative (**D**) mechanism as shown in Fig. 4. Fig. 4(b) shows an intermediate complex of reduced coordination for the NpO_2^+ ion; other monocations show similar characteristics. These results are consistent with those shown in Fig. 2.

3.3 Residence Times

Fig. 2 shows that the dynamics of water exchange varies for the different ions. To quantify the water exchange rate, a residence time correlation function, $R(t)$, was computed in the following manner[22,50,51]

$$\langle R(t)\rangle = \langle \frac{1}{N_0}\sum_{i=1}^{N_0} P_i(t,t^*)\rangle \qquad (3)$$

where N_0 is the total number of water molecules in the first hydration shell of the actinyl ion at time $t=0$. $P_i(t,t^*)$ is the Heaviside function, which is 1 if the i^{th} water molecule at time t is correlated with the i^{th} water molecule at time 0. We use the following operational definition of correlation[51]. If the i^{th} water molecule continuously resides in the first solvation shell between time 0 and time t, or it leaves the first solvation shell for a period not more than t^*, then it is correlated and $P_i(t,t^*)=1$. Otherwise, $P_i(t,t^*)=0$. The parameter t^* is taken to be 0.5 ps, in keeping with common practice[22,52–54]. The first hydration shell is defined as the first minimum of the RDF (see Fig. 4 of Pomogaev et al.[28]) between the An atom and the oxygen atom of water ($An\cdots O_w$) plus a small allowance to accommodate small radial movement of water molecules. The resulting first hydration shell distances were taken to be 0.30 nm for all dications and 0.34 nm for all monocations except AmO_2^+, for which 0.345 nm was used.

The residence time of water about an ion, τ, was obtained by numerically integrating $\langle R(t)\rangle$ with respect to time t. Average residence times and standard deviations were obtained from five independent simulations for each actinyl ion. Results are shown in Table 2.

Table 2 Residence times (τ) of SPC/E water molecules around AnO_2^{n+} in the first hydration shell. Activation free energies ($\Delta G^{\ddagger}$) are also shown. Subscripts are uncertainties in the last digit(s)

AnO_2^{n+}	τ (ns)	$\Delta G^{\ddagger}$ (kJ/mol)
UO_2^{2+}	0.77_5	21.0_1
NpO_2^{2+}	1.9_2	23.2_2
PuO_2^{2+}	18_6	28.7_8
AmO_2^{2+}	26_4	29.7_4
UO_2^+	2.0_2	23.4_2
NpO_2^+	1.87_5	23.2_1
PuO_2^+	1.04_3	21.7_1
AmO_2^+	0.169_4	17.2_1

Trends of residence time for mono- and dication actinyls can be understood in terms of the exchange mechanisms described in the previous section. For di-cations, which follow an associative interchange mechanism, residence time is strongly dependent on the angle bending constant (k_θ) of the actinyl ion. Since the incoming water molecule comes from near the apical "yl" oxygen atoms of the ion (Fig. 3(b)), ions having softer or more flexible bond angles will have faster water exchange.

To examine the sensitivity of exchange dynamics and solvation free energies on the O-U-O bond angle stiffness as well as the non-bonded interactions between water and UO_2^{2+}, we performed additional simulations on UO_2^{2+} in SPC/E water using two different sets of non-bonded Lennard-Jones parameters and charges. The non-bonded parameters proposed by Pomogaev et al.[28] and used in the present study will be referred to as Model 1, while the non-bonded parameters recommended by Kerisit et al.[21] will be referred to as Model 2. Furthermore, to study the sensitivity of the results to the stiffness of the O-U-O bond angle, we simulated both Model 1 and Model 2 with the harmonic force constant proposed by Pomogaev et al.[28] (k_θ = 198 kJ mol $^{-1}$ rad^{-2}) and the stiffer angle bending constant (k_θ= 1255 kJ mol^{-1}rad^{-2}) recommended by Wipff and co-workers[42]. Table 3 shows the results. Model 1 gives a first hydration shell radius of 0.246 nm, while Model 2 predicts a tighter radius of 0.236 nm. These predictions bracket the experimental value of 0.241-0.242 nm and there is no dependence on the O-U-O bond angle stiffness. The computed hydration free energies $\Delta G_{\rm hyd}$ are less negative for Model 1 than for Model 2, consistent with the hydration radii; Model 2

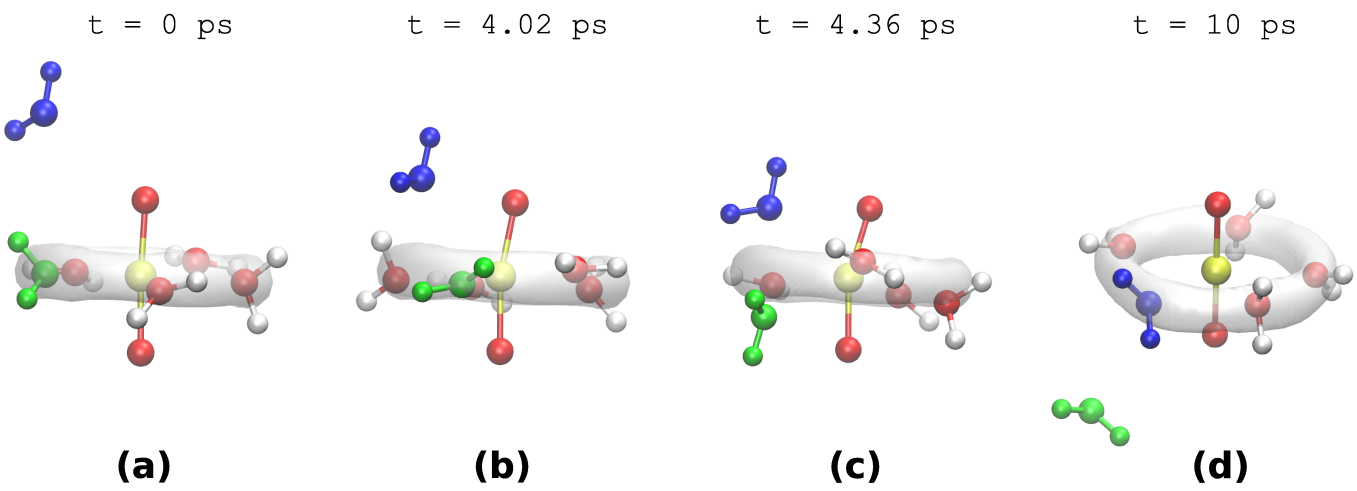

Fig. 3 Equatorial water exchange mechanism for UO_2^{2+} (other dications show similar behavior). Water molecules not involved in the first hydration shell are not shown for clarity. The gray ring around UO_2^{2+} represents the spatial extent of the first hydration shell. (a) and (b) UO_2^{2+} with five water molecules in its first hydration shell. The entering and leaving water molecules are colored blue and green, respectively. (c) Intermediate UO_2^{2+} with six waters in the first hydration shell, characteristic of an associative interchange ($\mathbf{I_a}$) exchange mechanism. The exchanging water molecules are approximately 0.27 nm from the central U atom, which is more than the nominal coordination distance 0.246 nm but less than the radius of the first solvation sphere (0.30 nm). Notice that the UO_2^{2+} ion is bent in this state. (d) The green water molecule leaves the first hydration shell while the blue water molecule takes its place and water exchange is complete.

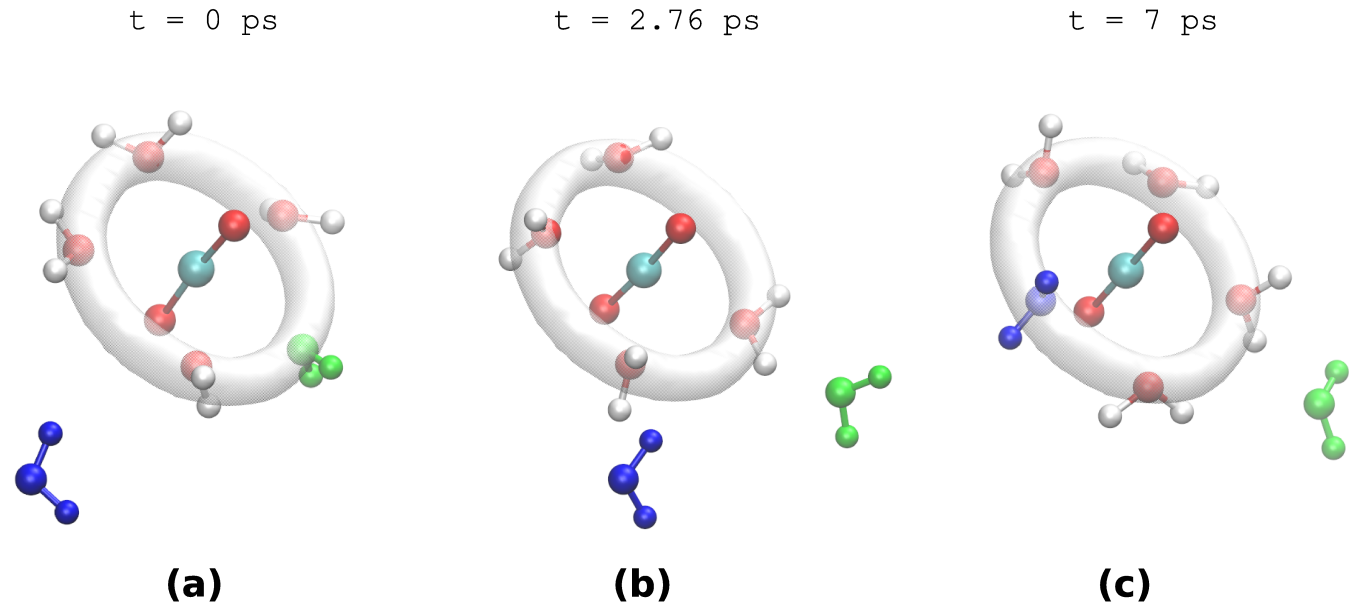

Fig. 4 Equatorial water exchange mechanism for NpO_2^+ (other monocations show similar behavior). Water molecules not involved in first hydration shell are not shown for clarity. The gray ring around NpO_2^+ represents the spatial extent of the first hydration shell. (a) NpO_2^+ with five water molecules in its first hydration shell with the blue water molecule approaching to replace the green water molecule. (b) The green water has left the first hydration shell and NpO_2^+ with four waters in its first hydration shell indicating a dissociative (**D**) exchange mechanism[8]. (c) The blue water molecule has joined the first hydration shell and water exchange is complete.

binds water more strongly than Model 1. Hydration free energies do not depend upon the stiffness of the O-U-O bond angle. To better enable comparison with experimental hydration free energies, our calculations include correction terms for interfacial effects[27,55,56], while these terms were not included in the work of Kerisit et al.[21], which is why there is a small difference between our calculated value and theirs for Model 2 with the stiff bond angle. Experimental hydration free energies vary widely and so it is not possible to identify which set of parameters best match experimental data, but certainly the present model yields reasonable values.

Water residence times and the associated Gibbs free energy of activation depend on both the non-bonded model parameters and the bond angle stiffness. The water exchange rate constant, which is the inverse of residence time, is related to the Gibbs free energy of activation ($\Delta G^{\ddagger}$) by the Eyring equation[57]:

$$\tau^{-1} = k_{\mathrm{ex}} = \frac{k_{\mathrm{B}}T}{h}\exp(\frac{-\Delta G^{\ddagger}}{RT}) \quad (4)$$

Water exchanges more slowly with Model 2 parameters than Model 1 parameters because of stronger water-UO_2^{2+} binding. The stiffness of the O-U-O bond angle has an even more pronounced effect on exchange dynamics; the stiffer bond angle significantly slows down water exchange. We were unable to observe a single water exchange event using Model 2 with the stiff bond angle over the course of a 150 ns simulation, while for the other models exchange was observed to occur on times scales ranging from 0.77-30 ns. For those cases in which exchanges were observed, the $\mathbf{I_a}$ mechanism was dominant, indicating that the mechanism of water exchange is insensitive to the particular force field parameters used here. Computed Gibbs free energies of activation vary from 21-38 kJ/mol, with Model 2 and the stiff bond angle agreeing best with available experimental data. It is interesting to note, however, that neither the stiff bond angle nor the potential energy surface corresponding to Model 2 agree with recent quantum mechanical calculations involving UO_2^{2+} explicitly interacting with water[28]. As shown in Table 3, the experimental $U\cdots O_w$ distance is 0.241-0.242 nm[23–26], which is slightly overestimated by Model 1 (0.246 nm) and slightly underestimated by Model 2 (0.236 nm). While the differing bond lengths affect calculated hydration free energies, exchange rates are insensitive to the $U\cdots O_w$ bond length. The results also show that the stiffness of the O-U-O bond angle, as characterized by k_θ, does impact the water exchange dynamics.

The main conclusion from these calculations is that the stiffness of the O-An-O bond angle in dication actinyls has a large effect on water exchange dynamics; the stiffer the angle bending potential, the longer will be the residence time. The k_θ values used in the MD simulations reported here for dication actinyls of U, Np, Pu, and Am are 198, 236, 602, and 791 kJmol^{-1}rad^{-2}, respectively[28]. The residence times reported in Table 2 follow the trend of increasing residence time down the series as the bond angle gets stiffer.

For monocations, which follow a dissociative exchange mechanism, water residence time is independent of k_θ. Instead, residence time depends on how weakly the water in the first hydration shell is bonded to the actinyl ion, i.e. how easily a water molecular can just move away from the first hydration shell. In other words, residence time depends on the $An\cdots O_w$ distance. The greater the $An\cdots O_w$ distance, the weaker will be the interaction between An and water and the easier it will be for water to leave the first hydration shell. This suggests that residence times should be inversely related to $An\cdots O_w$ distance. The $An\cdots O_w$ distances in nm for the monocation actinyls of U, Np, Pu, and Am were found to be 0.254, 0.254, 0.256, and 0.258, respectively[28]. The residence times reported in Table 2 follow the trend of decreasing residence time down the series.

The dynamics of water exchange with actinide cations has been the subject of extensive investigations, both experimentally[1,17,18,49] and computationally.[8,12,14–16,21,22,60,61] Most studies have focused on UO_2^{2+}, though some experimental studies have also been carried out on NpO_2^{2+} and PuO_2^{2+}.[18] Ikeda et al.[17] and Bardin et al.[18] studied the water exchange mechanism using proton NMR with mixed water-acetone solutions. The solutions were cooled to low temperatures (−50 to −95 °C) because the exchange dynamics at room temperature were too fast to detect. By extrapolating low temperature data of Ikeda et al.[17,49], Farkas et al.[1] estimated the water exchange rate for UO_2^{2+} to be 1.4×10^6 s^{-1} at 25 °C. Farkas et al.[1] used ^{17}O NMR to study the water exchange with UO_2^{2+}. They determined the rate constant for exchange between bound and free water to be 1.3×10^6 s^{-1} at 25 °C, consistent with the proton NMR data of Ikeda et al. Bardin et al.[18] have reported water exchange rate with UO_2^{2+} of the order of 10^4 s^{-1}, which appears slightly out of line compared to other experimental results. Bardin et al.[18] also measured the rate constants for water exchange with NpO_2^{2+} and PuO_2^{2+} and found them to be of the order of 10^6 s^{-1} and 10^4 s^{-1}, respectively.

In contrast to the experimental results, most previous theoretical / simulation studies predict much faster exchange dynamics for water and UO_2^{2+} at ambient conditions. For example, Vallet et al.[8] used quantum mechanical calculations to estimate the activation energy for associative (**A**) and interchange (**I**) mechanisms and predicted an exchange rate constant on the order of 10^8 s^{-1}. Hagberg et al.[14] performed MD simulations of UO_2^{2+} in water with their NEMO potential[62] and observed two instances of water exchange during a relatively short (10^{-10} s) simulation. Kerisit et al.[22] performed MD simulations of UO_2^{2+} in water using Wipff's potential[41,42] for the cation and the SPC/E model for water, and obtained an exchange rate constant equal to 8.1×10^8 s^{-1}. Frick et

Table 3 Effect of angle bending constant (k_θ) on residence time (τ) for UO_2^{2+}. Activation free energy ($\Delta G^\ddagger$) calculated from τ and hydration free energies of UO_2^{2+} (ΔG_{hyd}) at 298 K are also shown.

Model set[a]	k_θ (kJ mol^{-1}rad^{-2})	U$\cdots$O$_w$ distance (nm)	τ (ns)	$\Delta G^\ddagger$ (kJ mol^{-1})	ΔG_{hyd} (kJ mol^{-1})
1	198	0.246	0.77	21	-1390[28]
1	1255	0.246	30	31	-1390
2	198	0.236	1.2	28	-1685
2	1255	0.236	670[b]	38	-1552[21], -1685[Present work]
Experiments	NA	0.241[23,25,26]	760[1]	38[1]	-1360 ± 24 to -1665 ± 65[27,58,59]
		0.242[24]			

[a] $\{\sigma_{UU}, \varepsilon_{UU}, \sigma_{OUOU}, \varepsilon_{OUOU}, Q_U, Q_{OU}\}$ are $\{0.295, 0.530, 0.383, 0.057, 2.5, 0.25\}$ and $\{0.28508, 0.50208, 0.311814, 0.8368, 3.25, -0.625\}$ for Model 1[28] and Model 2[21], respectively. Units of σ, ε and charges are nm, kJ mol^{-1} and e, respectively.
[b] Calculated by Kerisit et al.[21] using a metadynamics technique. No exchange was observed in our 150 ns MD simulation.

al.[63] using a hybrid quantum / classical model did not observe any exchange, but their simulation was extremely short (8 ps). Similarly, Nichols et al.[61], using first principle molecular dynamics simulations, did not observe any exchange during extremely short simulations of 22 ps and 9 ps with 64 and 122 water molecules, respectively. Using the model of Pomogaev et al.,[28], we computed a water exchange time constant of 0.77 ns for UO_2^{2+}, which translates to a rate constant of 1.3×10^9 s^{-1}. This is much faster than the NMR data suggest. Recently, Kerisit et al.[21] developed a new model for classical simulation of UO_2^{2+} in water that yields exchange dynamics more in line with the experimental NMR results. However, this model tends to underestimate the size of the first hydration shell for UO_2^{2+} and does not reproduce the water-UO_2^{2+} potential energy surface or the U-O bond stretching frequency found in quantum calculations[28,64] and experiments.[64,65]

Why do so many of the theoretical / simulation studies predict faster exchange rates than the NMR data? Most of the quantum calculations mentioned above compute free energies of activation for particular configurations of bound and unbound water, and estimate exchange rate constants via eq. 4. Because these studies typically utilize a small number of water molecules and embed the system in some sort of continuum solvation model, there is often wide variation in the estimated activation free energies depending on the reaction coordinate, level of theory used, and the choice of solvation model. For example, Tsushima et al.[16] calculated the Gibbs free energy of activation $\Delta G^\ddagger = 42.4$ kJ/mol for one particular associative pathway, but found that the free energy barrier for a different associative pathway was 19.9 kJ/mol. It is stated that the accuracy of this method is 10 kJ/mol "at best". It is also pointed out that the large number of local minima in this system means that it is hard to be sure if the actual reaction coordinate corresponds to the minimum free energy pathway, and that molecular dynamics or Monte Carlo sampling might be needed. A study by Rotzinger[15] estimated a value of $\Delta G^\ddagger = 39.3$ kJ/mol and 27 kJ/mol for CAS-SCF(12/11)-PCM and CAS-SCF(12/11)-SCRF geometries, respectively. Vallet et al.[8] calculated the energy of activation $\Delta U^\ddagger = 19$ kJ/mol and 38 kJ/mol for **A** and **I** mechanisms, respectively. In an effort to account for solvation effects more explicitly, Bühl et al.[12] calculated the Helmholtz free energy of activation for the associative exchange of water and UO_2^{2+} using ab initio molecular dynamics and thermodynamic integration. They estimated that the Helmholtz free energy barrier for exchange was $\Delta A^\ddagger = 28$ kJ/mol, a value that they noted was "noticeably lower than the experimental free energy barrier" of 38 kJ/mol. They attributed this underestimation of the free energy barrier to deficiencies in the density functional theory functionals employed and also the possibility that the relatively short simulation times afforded by their methods could have led to insufficient sampling. Given the exponential dependence of the water exchange rate on the free energy barrier, small energy barrier differences on the order of 10 kJ/mol can lead to extremely large differences in rate constants.

Using the model of Pomogaev et al.[28] along with a system of 1000 water molecules and a single cation, we find exchange rates between the first and second solvation shells that are much faster than the experimental NMR results[1], as shown in Table 3. Interestingly, however, computed coordination numbers and the observed exchange mechanism agree with previous computational and experimental studies. It is also interesting that the fast exchange rate predicted here is consistent with several of the previous theoretical studies that found lower free energy barriers than that measured with NMR. While a difference of three orders of magnitude between experimental and simulated rate constants is quite large, it is important to recall that this corresponds to a mere difference of 10-17 kJ/mol of activation free energy as shown in Table 3. This emphasizes how small energy differences can yield large differences

in rates. We can think of at least three possible explanations for these observations. First, the NMR experiments record the exchange between water that is associated with the cation and water that is in the bulk. The simulations all consider the exchange dynamics between the first and second coordination shells of the cation. Even in the second coordination shell, however, water still experiences interactions with the cation and cannot be considered to be residing in "bulk" water. Thus the simulations may only be capturing the first part of the exchange process, while the ultimate exchange with the bulk captured by NMR takes longer time. However, Nichols et al.[61] using first principle molecular dynamics simulations found the exchange rate on the order of picoseconds for water exchange between the second hydration shell and bulk water, thereby suggesting that this is not the rate limiting step. A second, albeit unlikely, explanation for why NMR exchange dynamics are slower than that predicted by simulations is that the high magnetic fields associated with the NMR experiments could impact the vibrational frequency of UO_2^{2+}. We showed that as the O-U-O bond angle becomes stiffer, water exchange dynamics become slower. It has been observed that large magnetic fields perturb the vibrational frequencies of molecules[66–84] and this could result in a distortion of the exchange dynamics measured with NMR. The third explanation is that the models used in the simulations are simply not sophisticated enough to capture the dynamical exchange process between water and UO_2^{2+} and need to be improved. If this is the case, then the present study can serve as a benchmark for further studies aimed at systematically improving water-actinide force fields.

3.4 Effect of Water Models on Dynamics

All of the results presented above were for simulations carried out with the extended simple point charge (SPC/E) model of water. There are a number of different water models commonly used besides the SPC/E model, however, so to investigate the sensitivity of the results to variations in water model, simulations were carried out for UO_2^{2+} in four other water molecules: SPC/Fw, TIP3P, TIP4P, and TIP5P. Note that a "hybrid" UO_2^{2+} model was used, as described elsewhere[28]. Results are presented in Table 4. The neat water diffusivities for the different models are in agreement with literature values[30]. The self-diffusivities of UO_2^{2+} in the different water models vary substantially. Self-diffusivities range from $0.52 \times 10^{-9} m^2 s^{-1}$ for UO_2^{2+} in SPC/Fw water to $1.5 \times 10^{-9} m^2 s^{-1}$ in TIP3P water. These trends follow the trends in diffusivity for neat water; the uranyl ion diffuses fastest in the water model having the highest water diffusivity. To show this, we computed the ratio of the ion self-diffusivity and the neat water self-diffusivity for each model. The ratios are essentially equal at around 0.25. By comparing the self-diffusivity of water with the actinyl ions present and in the neat state, it is evident that dilute actinyl ions have no significant effect on the diffusivity of water.

Further, the residence times of water in the first hydration shell of UO_2^{2+} for the different water models have also been computed. Since the incoming water that replaces a coordinated water for dication actinyls comes from near the "yl" oxygen, rapid exchange is favored by a stronger attraction between the "yl" oxygen (OAn) and the oxygen of water (Ow). This is reflected in the residence times shown in Table 4, where the effect of Lennard Jones parameters ε_{OAn-Ow} used in the simulations have been compared with the computed residence times. A smaller ε_{OAn-Ow} means a higher residence time and vice versa. A minor exception to this rule is observed with the TIP3P water model, which we suspect is due to the fact that it has a significantly larger water self-diffusivity than the other models (see Table 4), which facilitates exchange.

4 Conclusions

A classical force field for aqua actinyl cations (AnO_2^{n+}, An = U, Np, Pu, Am; n =1, 2), originally developed using quantum mechanical calculations and validated against static properties, has been used to compute the dynamical properties of water - actinyl ion systems. The computed self-diffusion coefficients of water and the cations are in agreement with those from direct experimental studies. The diffusion coefficients of dications are somewhat smaller than that of monocations, which is attributed to the greater affinity between water and the dications. Two different types of water exchange mechanisms were observed: associative interchange ($\mathbf{I_a}$) for dications and dissociative exchange (**D**) for monocations. The $\mathbf{I_a}$ mechanism for the dications has been observed in other studies as well. We find that the rate of water exchange is sensitive to the stiffness of the O-An-O bond angle, with a stiffer bond angle resulting in slower water exchange. Water exchange was fastest for UO_2^{2+} and slowest for AmO_2^{2+}. In contrast, for the monocations which follow a dissociative mechanism, the rate of water exchange is related to the strength of the non-bonded interactions between water and the actinyl ion. Thus water exchange is fastest for AmO_2^{+} and slowest for UO_2^{+}. The computed residence times for water in the first hydration shell of UO_2^{2+} are significantly shorter than those reported in NMR studies, but agree with many previous computational studies of water exchange free energy barriers. The reason for the discrepancy between simulations and experiment is not clear, but several possible explanations are given. Finally, we note that there is a long history of empirically adjusting classical force field parameters to match some sub-set of experimental data. In this work, we tested whether a single classical force field, derived from *ab initio* simulations, can simultaneously capture both static and dynamic properties of aqua

Table 4 Diffusion coefficients (D, $10^{-9}m^2s^{-1}$) of UO_2^{2+} and water, average number of water molecules in the first solvation shell (N_w^{fs}), and residence times (τ) for different water models. Subscripts are uncertainties in the last digit(s)

Water model	$D_{UO_2^{2+}}$	$D_{UO_2^{2+}}/D^a_{water}$	D_{water}	D^a_{water}	N_w^{fs}	ε_{OAn-Ow} (kJ/mol)	τ (ps)
SPC/E	0.61_9	0.25	2.45_4	2.51_3	5.0067_3	0.192	770_{50}
TIP4P	1.0_2	0.29	3.39_3	3.50_7	5.0254_3	0.850	186_4
SPC/Fw	0.52_3	0.26	2.03_6	2.03_4	5.0897_8	1.080	159_3
TIP3P	1.5_2	0.28	5.45_8	5.44_7	5.35_1	1.080	42.0_2
TIP5P	0.72_9	0.27	2.67_5	2.69_3	6.436_3	1.470	43.0_5

[a] in neat water.

actinyl ions. The force field performs reasonably well in capturing qualitative trends as well as most quantitative dynamic and static properties, with the notable exception of the rate constant for water exchange. To date, we know of no classical force field for actinyl ions and water that simultaneously captures all known experimental properties of this system and is consistent with potential energy surfaces derived from high-level quantum calculations. This suggests that more sophisticated force fields may be necessary to more accurately model these systems.

5 Acknowledgements

This work was supported by Materials Science of Actinides, an Energy Frontier Research Center funded by the U.S. Department of Energy, Office of Science, Office of Basic Energy Sciences under award number DE-SC0001089. Computational resources were provided by University of Notre Dame Center for Research Computing and the National Energy Research Scientific Computing Center (NERSC).

References

1 I. Farkas, I. Bányai, Z. Szabó, U. Wahlgren and I. Grenthe, *Inorg. Chem.*, 2000, **39**, 799–805.
2 D. M. H. Kern and E. F. Orlemann, *J. Am. Chem. Soc.*, 1949, **71**, 2102–2106.
3 G. Marx, R. Gauglitz, V. Friehmelt and K. Feldner, *J. Less-Common Met.*, 1986, **122**, 185–188.
4 R. D. Brown, W. B. Bunger, W. L. Marshall and C. H. Secoy, *J. Am. Chem. Soc.*, 1954, **76**, 1580–1581.
5 R. D. Brown, W. B. Bunger, W. L. Marshall and C. H. Secoy, *J. Am. Chem. Soc.*, 1954, **76**, 1532–1535.
6 G. Marx and H. Bischoff, *J. Radioanal. Chem.*, 1976, **30**, 567–581.
7 Y. Awakura, K. Sato, H. Majima and S. Hirono, *Metall. Trans. B*, 1987, **107**, 19–23.
8 V. Vallet, U. Wahlgren, B. Schimmelpfennig, Z. Szabó and I. Grenthe, *J. Am. Chem. Soc.*, 2001, **123**, 11999–2008.
9 V. Vallet, T. Privalov, U. Wahlgren and I. Grenthe, *J. Am. Chem. Soc.*, 2004, **126**, 7766–7.
10 S. Doudou, K. Arumugam, D. J. Vaughan, F. R. Livens and N. A. Burton, *Phys. Chem. Chem. Phys.*, 2011, **13**, 11402–11.
11 M. Bühl, R. Diss and G. Wipff, *J. Am. Chem. Soc.*, 2005, **127**, 13506–13507.
12 M. Bühl and H. Kabrede, *Inorg. Chem.*, 2006, **45**, 3834–6.
13 M. Bühl, H. Kabrede, R. Diss and G. Wipff, *J. Am. Chem. Soc.*, 2006, **128**, 6357–6368.
14 D. Hagberg, G. Karlstrom, B. O. Roos and L. Gagliardi, *J. Am. Chem. Soc.*, 2005, **127**, 14250–14256.
15 F. P. Rotzinger, *Chem. Eur. J.*, 2007, **13**, 800–11.
16 S. Tsushima, *J. Phys. Chem. A*, 2007, **111**, 3613–3617.
17 Y. Ikeda, S. Soya, H. Fukutomi and H. Tomiyasu, *J. Inorg. Nucl. Chem.*, 1979, **41**, 1333 – 1337.
18 N. Bardin, P. Rubini and C. Madic, *Radiochim. Acta*, 1998, **83**, 189–194.
19 P. Wåhlin, V. Vallet, U. Wahlgren and I. Grenthe, *Inorg. Chem.*, 2009, **48**, 11310–3.
20 P. Wåhlin, B. Schimmelpfennig, U. Wahlgren, I. Grenthe and V. Vallet, *Theor. Chem. Acc.*, 2009, **124**, 377–384.
21 S. Kerisit and C. Liu, *J. Phys. Chem. A*, 2013, **117**, 6421–6432.
22 S. Kerisit and C. Liu, *Geochim. Cosmochim. Acta*, 2010, **74**, 4937–4952.
23 V. Vallet, U. Wahlgren, B. Schimmelpfennig, H. Moll, Z. Szabó and I. Grenthe, *Inorg. Chem.*, 2001, **40**, 3516–3525.
24 H. A. Thompson, G. E. Brown Jr and G. A. Parks, *Am. Mineral.*, 1997, **82**, 483–496.
25 P. G. Allen, J. J. Bucher, D. K. Shuh, N. M. Edelstein and T. Reich, *Inorg. Chem.*, 1997, **1669**, 4676–4683.
26 U. Wahlgren, H. Moll, I. Grenthe, B. Schimmelpfennig, L. Maron, V. Vallet and O. Gropen, *J. Phys. Chem. A*, 1999, **103**, 8257–8264.
27 N. Rai, S. P. Tiwari and E. J. Maginn, *J. Phys. Chem. B*, 2012, **116**, 10885–97.
28 V. Pomogaev, S. P. Tiwari, N. Rai, G. Goff, W. Runde, W. Schneider and E. Maginn, *Phys. Chem. Chem. Phys*, 2013, **15**, 15954–15963.
29 H. J. C. Berendsen, J. R. Grigera and T. P. Straatsma, *J. Phys. Chem.*, 1987, **91**, 6269–6271.
30 Y. Wu, H. L. Tepper and G. A. Voth, *J. Chem. Phys.*, 2006, **124**, 24503.
31 W. L. Jorgensen, J. Chandrasekhar, J. D. Madura, R. W. Impey and M. L. Klein, *J. Chem. Phys.*, 1983, **79**, 926.
32 M. W. Mahoney and W. L. Jorgensen, *J. Chem. Phys.*, 2000, **112**, 8910–8922.
33 B. Hess, C. Kutzner, D. van der Spoel and E. Lindahl, *J. Chem. Theory Comput.*, 2008, **4**, 435–447.
34 W. G. Hoover, *Phys. Rev. A*, 1985, **31**, 1695–1697.
35 J. E. Basconi and M. R. Shirts, *J. Chem. Theory Comput.*, 2013, **9**, 2887–2899.
36 W. Humphrey, A. Dalke and K. Schulten, *J. Mol. Graphics*, 1996, **14**,

33–38.
37 M. P. Allen and D. J. Tildesley, *Computer Simulation of Liquids*, Clarendon Press: Oxford, 1987.
38 I.-C. Yeh and G. Hummer, *J. Phys. Chem. B*, 2004, **108**, 15873–15879.
39 S. Tazi, A. Boan, M. Salanne, V. Marry, P. Turq and B. Rotenberg, *J. Phys.: Condens. Matter*, 2012, **24**, 284117.
40 E. Mauerhofer, K. P. Zhernosekov and F. Rösch, *Radiochim. Acta*, 2004, **92**, 5–10.
41 P. Guilbaud and G. Wipff, *J. Mol. Struct. THEOCHEM*, 1996, **366**, 55–63.
42 P. Guilbaud and G. Wipff, *J. Phys. Chem.*, 1993, **97**, 5685–5692.
43 J. R. Harris, *J. Phys. Chem. B*, 2010, **114**, 9572–9577.
44 C. H. Langford and H. B. Gray, *Ligand Substitution Processes*, WA Benjamin, Inc., 1966.
45 L. Helm and A. E. Merbach, *Chem. Rev.*, 2005, **105**, 1923–1959.
46 A. Merbach, *Pure Appl. Chem.*, 1982, **54**, 1479–1498.
47 A. E. Merbach, *Pure Appl. Chem*, 1987, **59**, 161–172.
48 K. Hermansson and M. Wojcik, 1998, **5647**, 6089–6097.
49 Z. Szabó, J. Glaser and I. Grenthe, *Inorg. Chem.*, 1996, **35**, 2036–2044.
50 R. W. Impey, P. A. Madden and I. R. McDonald, *J. Phys. Chem.*, 1983, **87**, 5071–5083.
51 E. Guardia and J. A. Padró, *J. Phys. Chem.*, 1990, **94**, 6049–6055.
52 T. S. Hofer, H. T. Tran, C. F. Schwenk and B. M. Rode, *J. Comput. Chem.*, 2004, **25**, 211–7.
53 A. Tongraar and B. M. Rode, *Chem. Phys. Lett.*, 2005, **403**, 314–319.
54 D. Laage and J. T. Hynes, *J. Phys. Chem. B*, 2008, **112**, 7697–701.
55 G. L. Warren and S. Patel, *J. Chem. Phys.*, 2007, **127**, 064509.
56 D. Horinek, S. I. Mamatkulov and R. R. Netz, *J. Chem. Phys.*, 2009, **130**, 124507.
57 H. Eyring, *J. Chem. Phys.*, 1935, **3**, 107.
58 J. K. Gibson, R. G. Haire, M. Santos, J. Marçalo and A. Pires de Matos, *J. Phys. Chem. A*, 2005, **109**, 2768–81.
59 Y. Marcus, *Ion Solvation*, John Wiley and Sons Ltd., 1985, pp. 107–125.
60 Z. Szabó, T. Toraishi, V. Vallet and I. Grenthe, *Coord. Chem. Rev.*, 2006, **250**, 784–815.
61 P. Nichols, E. J. Bylaska, G. K. Schenter, W. de Jong and W. D. Jong, *J. Chem. Phys.*, 2008, **128**, 124507.
62 O. Engkvist, P.-O. Åstrand and G. Karlström, *Chem. Rev.*, 2000, **100**, 4087–4108.
63 R. J. Frick, T. S. Hofer, A. B. Pribil, B. R. Randolf and B. M. Rode, *J. Phys. Chem. A*, 2009, **113**, 12496–12503.
64 A. O. Tirler, A. K. H. Weiss and T. S. Hofer, *J. Phys. Chem. B*, 2013, **117**, 16174–87.
65 R. D. Hunt and L. Andrews, *J. Chem. Phys.*, 1993, **98**, 3690.
66 T. Tamura, D. Kamikihara, Y. Maehara, N. Omura and K. Miwa, *Mater. Trans.*, 2007, **48**, 234–238.
67 R. Cai, H. Yang, J. He and W. Zhu, *J. Mol. Struct.*, 2009, **938**, 15–19.
68 T. Helgaker, M. Jaszuski and K. Ruud, *Chem. Rev.*, 1999, **99**, 293–352.
69 H. Hu, H. Hou and B. Wang, *J. Phys. Chem. C*, 2012, **116**, 19773–19780.
70 H. Inaba, T. Saitou, K.-i. Tozaki and H. Hayashi, *J. Appl. Phys.*, 2004, **96**, 6127.
71 N. Su and C.-F. Wu, *Cem. Concr. Compos.*, 2003, **25**, 681–688.
72 K. X. Zhou, G. W. Lu, Q. C. Zhou, J. H. Song, S. T. Jiang and H. R. Xia, *J. Appl. Phys.*, 2000, **88**, 1802.
73 L. Holysz, A. Szczes and E. Chibowski, *J. Colloid Interface Sci.*, 2007, **316**, 996–1002.
74 H. E. Lundager Madsen, *J. Cryst. Growth*, 2004, **267**, 251–255.
75 Y. Wang, B. Zhang, Z. Gong, K. Gao, Y. Ou and J. Zhang, *J. Mol. Struct.*, 2013, **1052**, 102–104.
76 F. Gutiérrez-Mejía and J. Ruiz-Suárez, *J. Magn. Magn. Mater.*, 2012, **324**, 1129–1132.
77 A. Szcześ, E. Chibowski, L. Holysz and P. Rafalski, *Chem. Eng. Process. Process Intensif.*, 2011, **50**, 124–127.
78 R. D. Ambashta and M. Sillanpää, *J. Hazard. Mater.*, 2010, **180**, 38–49.
79 K.-T. Chang and C.-I. Weng, *Comput. Mater. Sci.*, 2008, **43**, 1048–1055.
80 X. Pang and B. Deng, *Europhys. Lett.*, 2010, **92**, 65001.
81 X. Pang and B. Deng, *Sci. China Ser. G -Phys. Mech. Astron.*, 2008, **51**, 1621–1632.
82 A. Pazur and M. Winklhofer, *Geophys. Res. Lett.*, 2008, **35**, L16710.
83 I. Otsuka and S. Ozeki, *J. Phys. Chem. B*, 2006, **110**, 1509–12.
84 H. Hosoda, H. Mori, N. Sogoshi, A. Nagasawa and S. Nakabayashi, *J. Phys. Chem. A*, 2004, **108**, 1461–1464.